Baryons as solitonic solutions of the chiral sigma model

Wolfgang Bentz
Department of Physics, Faculty of Science, University of Tokyo, Hongo 7-3-1, Bunkyo-ku, Tokyo 113, Japan

Josef Hartmann and Friedrich Beck
Institut für Kernphysik, Technical University of Darmstadt, Schloßgartenstr. 9, D-64289 Darmstadt, Germany
(Received 28 June 1996)

Self-consistent solitonic solutions with baryon number one are obtained in the chiral quark sigma model. The translational invariant vacuum is stabilized by a Landau ghost subtraction procedure based on the requirement of the Källén-Lehmann (KL) representation for the meson propagators. The connection of this ghost free model (KL model) to the more popular Nambu-Jona-Lasinio (NJL) model is discussed in detail. [S0556-2813(96)01911-5]

PACS number(s): 14.20.Dh, 12.39.Fe, 12.39.Jh, 24.85.+p

I. INTRODUCTION

The development of effective models of QCD and their application to the structure of hadrons is an important and active field in contemporary medium energy physics. In most of these models, mesonic degrees of freedom, in particular pions, play an important role. This is based on the observation that, in the limit of a large number of colors, QCD reduces to an effective theory of mesons described by an effective action in terms of these variables [1]. Since this effective action reflects the underlying quark dynamics, it is natural to base effective models on a Lagrangian with quark and meson fields, and to integrate out the quark fields. This quark-meson theory should properly incorporate the chiral symmetry and its spontaneous breakdown, which are important features of low energy QCD. One of the first models of this kind, the Friedberg-Lee model [2,3] in its simplest form, involved just the isoscalar-scalar sigma meson. In order to incorporate chiral symmetry, one is naturally led to the linear sigma model which in addition includes the pion as a Goldstone boson [4]. The nucleon, which emerges as a soliton of the meson field equations, was investigated in the mean field approximation to this model [5]. First calculations, which neglected the contribution of the quark Dirac sea to the effective action, were actually quite successful [6].

If one attempts to include the effects due to the Dirac sea, it is natural to consider the fields and parameters of the linear sigma model, e.g.; the pion mass, as the ''physical'' (or ''dressed'') ones and to follow the standard renormalization treatment. It has been shown, however, that the renormalization procedure in the framework of the loop expansion leads to an instability of the translational invariant vacuum [7,8]. That is, the energy of the vacuum (without any valence quarks) can be lowered without bounds by increasing the high momentum components of the meson fields. This problem, which is common to all renormalized asymptotically nonfree theories [9], can be traced back to an unphysical Tachyon pole (the so called Landau ghost) of the meson propagators [10]. Since, contrary to quantum electrodynamics, in hadronic effective field theories this ghost pole occurs usually at rather low energies of the order of the baryon mass ($\simeq$1 GeV), the model as it stands cannot be applied consistently to hadron physics. Based on the working hypothesis that this difficulty is not inherent to the model itself but to the approximation scheme used (loop expansion), a method was proposed to construct a ghost free model within the loop expansion [11]. The essence of this approach, which is based on the work of Redmond and Bogoliubov *et al.* [12], is the construction of meson propagators which satisfy the Källén-Lehmann (KL) representation. In practice this amounts to the prescription to subtract the ghost pole term from the Schwinger-Dyson propagators, which should be regarded as forming part of the definition of the approximation used.[1] By considering the vacuum part of the effective mesonic action for fixed mesonic profiles, it has been shown recently [14] that this method can be applied successfully to finite solitons. The method has also been applied to assess higher loop effects in infinite systems [15].

The purpose of the present paper is twofold: First, we wish to establish the connection of the KL model discussed above to the more popular Nambu-Jona-Lasinio (NJL) model [16–20]. To establish a quantitative connection between both models on the one quark loop level, we will discuss the renormalization procedure in the σ model for finite cutoff Λ. The NJL model then emerges as a particular case of the sigma model if Λ is chosen such that $Z_M=0$,[2] where Z_M is the wave function renormalization constant for the mesons.

[1]The ghost eliminated sigma model will be called the KL (for Källén-Lehmann) model from now on. We note that, besides simply ignoring the effect of the Dirac sea [5,6], there exist also other possibilities to avoid the Landau ghost, for example, the method proposed in [13], or the use of a sufficiently low momentum cutoff like in the NJL model. The connection to this second possibility will be discussed in detail in later sections.

[2]In this case the original meson-quark Lagrangian does not involve derivatives of the meson fields (Φ), in which case these fields can be eliminated immediately due to the Euler-Lagrange equations $\partial\mathcal{L}/\partial\Phi=0$. There exist many investigations on this equivalence or compositeness condition $Z_M=0$, see for example, [21,22]. Our interest here is somewhat different: We consider the cutoff Λ as a physical parameter characterizing the effective theory, and the condition $Z_M=0$ is imposed on Λ for fixed renormalized coupling constants.

This particular cutoff Λ_c also characterizes the onset of the Landau ghost, that is, for $\Lambda>\Lambda_c$ the ghost subtraction must be performed to obtain the physical KL model. The second purpose of this paper is to present self-consistent soliton solutions in the KL model and to compare them to those of the NJL model. As a first step, we will restrict our numerical investigations to the case where the meson fields are restricted to the chiral circle, but simple arguments (see Sec. III) strongly indicate that stable solutions exist also without this fixation. We will also restrict our discussion to the Hedgehog configuration, leaving the projection onto physical baryon states and the calculation of observables for future work.

II. EFFECTIVE MESONIC ACTION AND VACUUM INSTABILITY

In this section we discuss the effective mesonic action and its behavior for large and small soliton sizes in the σ model. The ghost subtraction will be introduced to stabilize the vacuum, and the connection to the NJL model will be established.

A. Effective action in the σ model

If the parameters $\mu^2(<0)$ and λ^2, which characterize the shape of the ''Mexican hat'' potential in the linear σ model [4], are expressed by the ''physical'' parameters m_σ and m_π, the Euclidean Lagrangian takes the form[3] $\mathcal{L}=\mathcal{L}_F+\mathcal{L}_M+\mathcal{L}_{\rm SB}$ with $\mathcal{L}_F=\bar\psi(-i\partial\!\!\!/+MU)\psi$, and

$$\mathcal{L}_M=\frac{v^2}{2}[(\partial_\mu U)(\partial_\mu U^+)+\tfrac{1}{4}(m_\sigma^2-m_\pi^2)(U^+U-1)^2 + m_\pi^2(U^+U-1)]. \tag{2.1}$$

Here ψ is the flavor SU(2) quark field, $U=(1/v)(\sigma+i\gamma_5\boldsymbol{\pi}\cdot\boldsymbol{\tau})$ is the chiral field, v is the vacuum expectation value of σ, and $M=gv$ is the effective (constituent) quark mass. The term $\mathcal{L}_{\rm SB}=c\sigma$ breaks the chiral symmetry explicitly. If we renormalize the pion propagator at zero momentum, as will be done below, then [23] $c=vm_\pi^2$ and $v=f_\pi$, where m_π and f_π are defined at zero momentum. The parameters of the model are g (or M), m_σ, m_π and the ultraviolet cutoff Λ, which can be left finite or eventually sent to infinity. After introducing a chemical potential which is adjusted to give a $B=1$ state [17], and integrating out the quark fields in the generating functional, we obtain the following effective mesonic action [7,17]:

$$\Gamma=\overline{\Gamma_F}+\text{c.t.}+\Gamma_M+\Gamma_{\rm SB}+\Gamma_{\rm val} \equiv\Gamma_{\rm vac}+\Gamma_{\rm val}. \tag{2.2}$$

Here

$$\overline{\Gamma_F}=-\tfrac{1}{2}\ \mathrm{Tr}\ \ln(1+GV) \tag{2.3}$$

is the unrenormalized quark vacuum loop contribution with $G=(-\partial^2+M^2)^{-1}$, and

$$V=iM\partial\!\!\!/U+M^2(U^+U-1). \tag{2.4}$$

The mesonic parts are given by $\Gamma_M=\int d^4x\mathcal{L}_M$, $\Gamma_{\rm SB}=\int d^4x\mathcal{L}_{\rm SB}$, and the valence quark part $\Gamma_{\rm val}$ is given, for example, in [17].

The counter terms (c.t.) in Eq. (2.2) are determined such that in a derivative expansion of the renormalized fermion loop contribution $\Gamma_F=\Gamma_F+$c.t. no terms of the same form as those already present in Γ_M appear. In particular, this means that the quark loop should give no contributions quadratic in the meson fields and their derivatives, which corresponds to the choice of the renormalization point $\mu_r^2=0$ for the meson masses and wave functions. The counterterms therefore take the form

$$\text{c.t.}=\tfrac{1}{2}\ \mathrm{Tr}\ GV-\tfrac{1}{4}\mathrm{Tr}\ G^2V^2. \tag{2.5}$$

For later developments, we give the explicit forms of the counterterms as obtained in a continuous plane wave basis:

$$\tfrac{1}{2}\ \mathrm{Tr}\ GV=\frac{v^2}{2}\,\delta m_\pi^2\int d^4x(U^+U-1), \tag{2.6}$$

$$-\tfrac{1}{4}\ \mathrm{Tr}\ G^2V^2=\frac{v^2}{2}(Z_M-1)\int d^4x[(\partial_\mu U)(\partial_\mu U^+) + M^2(U^+U-1)^2], \tag{2.7}$$

where we have defined

$$\delta m_\pi^2=8N_Cg^2\overline{F_1},\quad Z_M=1-4N_Cg^2\overline{F_2} \tag{2.8}$$

with[4]

$$\overline{F_n}=\int_{\rm reg}\frac{d^4k}{(2\pi)^4}\frac{1}{(k^2+M^2)^n}\quad(n=1,2). \tag{2.9}$$

If the counterterms (2.6) and (2.7) are added to the mesonic action, we obtain

$$\Gamma=\overline{\Gamma_F}+\frac{v^2}{2}\int d^4x\{Z_M(\partial_\mu U)(\partial_\mu U^+)+\tfrac{1}{4}[m_\sigma^2-m_\pi^2 +4M^2(Z_M-1)](U^+U-1)^2 +(m_\pi^2+\delta m_\pi^2)(U^+U-1)\}+\Gamma_{\rm SB}+\Gamma_{\rm val} =\Gamma_{\rm vac}+\Gamma_{\rm val}. \tag{2.10}$$

As expected, the counterterms (2.5) give rise to a factor Z_M in the kinetic term, and the masses are replaced according to $m_\alpha^2\to m_\alpha^2+\delta m_\alpha^2$ $(\alpha=\sigma,\pi)$ with δm_π^2 given in Eq. (2.8), and $\delta m_\sigma^2-\delta m_\pi^2=4M^2(Z_M-1)$. One can easily confirm that

[3] In Euclidean metric, $x_\mu=x^\mu=(\tau,\mathbf{r})$ with $\tau=ix^0$, $0<\tau<T$, and $\gamma_\mu=\gamma^\mu=(i\beta,\boldsymbol{\gamma})$. We also use the notation $\mathrm{Tr}\,A\equiv N_C\int d^4x\ \mathrm{tr}\langle x|A|x\rangle$, where $N_C=3$ and tr refers to the Dirac and isospin indices. The fermionic determinant is assumed to be regularized in some scheme. To avoid the explicit reference to a particular regularization scheme, we employ the symbolic notation in Eq. (2.3).

[4] Here, and in the following, the notation reg indicates that the loop integral is regularized in some scheme.

these counterterms Z_M, δm_π^2 and δm_σ^2 are just those which follow from the one quark-loop self-energies of the mesons.

For the numerical evaluation of the total energy $E=(1/T)\Gamma$, to be discussed in Sec. III, it is, however, more appropriate to add the counterterms (2.5) to the unrenormalized quark loop rather than to the mesonic terms, i.e., to evaluate the renormalized quark loop contribution $\Gamma_F=\Gamma_F+$c.t. in one common basis. We will use the basis of Kahana and Ripka [27]. The resulting form of the vacuum energy in this basis is given in [7,14] and will not be reproduced here.

B. Behavior for large and small sizes

Let us now discuss the behavior of the vacuum part ($\Gamma_{\rm vac}$) of Eq. (2.10) for large and small sized localized meson fields. To simplify the discussion, in this subsection we will refer to the chiral symmetric ($c=m_\pi=0$) nonlinear (nl) model,[5] where $\sigma^2+\boldsymbol{\pi}^2=v^2$. This leaves only the kinetic term ($\Gamma_{\rm kin}$) in the mesonic part of Eq. (2.10):

$$\Gamma_{\rm nl,vac}=\overline{\Gamma_F}+Z_M\Gamma_{\rm kin}=\Gamma_F+\Gamma_{\rm kin}. \tag{2.11}$$

$$\Gamma_F=\overline{\Gamma_F}+(Z_M-1)\Gamma_{\rm kin}. \tag{2.12}$$

We assume for the moment that the fields depend only on the dimensionless variable $\mathbf{x}=\mathbf{r}/R$ where R characterizes the spatial extension of the fields. Then $\Gamma_{\rm kin}\propto R$, see Eq. (2.20) below. The behavior of the quark loop term is most easily seen by expanding Eq. (2.3) in powers of V, which leads to an expansion in terms of n-point functions. The general expression is given in Appendix A, and for the nonlinear model, where only the first term of Eq. (2.4) contributes, it reduces to[6]

$$\frac{1}{T}\Gamma_F=N_C\sum_{n=2}^{\infty}R^{3-n}\frac{(-1)^n}{2n}\int\frac{d^3t_1}{(2\pi)^3}\cdots\frac{d^3t_{n-1}}{(2\pi)^3}\,{\rm tr}[V_1(\mathbf{t}_1)\cdots V_1(\mathbf{t}_n)](\overline{F_n}(Q_1,\ldots,Q_{n-1})|_{Q_i=(0,\mathbf{t}_i/R)}-\delta_{n2}\overline{F_2}). \tag{2.13}$$

Here $\mathbf{t}$ is the dimensionless momentum variable corresponding to $\mathbf{x}$ (i.e., $\mathbf{t}=\mathbf{p}R$), and $\mathbf{t}_n\equiv-(\mathbf{t}_1+\cdots+\mathbf{t}_{n-1})$.

$$V_1(\mathbf{t})=g\boldsymbol{\gamma}\cdot\mathbf{t}[s(\mathbf{t})+i\boldsymbol{\pi}(\mathbf{t})\cdot\boldsymbol{\tau}\gamma_5] \tag{2.14}$$

is the Fourier transform of the first term in Eq. (2.4) with $s(\mathbf{x})\equiv\sigma(\mathbf{x})-v$ the shifted field, and the unrenormalized n-point functions are defined by

$$\overline{F_n}(Q_1,\ldots,Q_{n-1})=\int_{\rm reg}\frac{d^4K}{(2\pi)^4}\frac{1}{[K^2+M^2][(K+Q_1)^2+M^2]\cdots[(K+Q_1+\cdots+Q_{n-1})^2+M^2]}. \tag{2.15}$$

The subtraction term in Eq. (2.13) is due to the wave function renormalization in Eq. (2.12), see Eqs. (2.8) and (2.20) below. We will denote the renormalized two-point function by

$$F_2(Q)=\overline{F_2}(Q)-\overline{F_2}. \tag{2.16}$$

The higher n-point functions are finite and not changed by renormalization, i.e., $F_n=F_n$ for $n>2$.

The behavior for large R is determined by the long wavelength behavior of the n-point functions in Eq. (2.13). Since $F_2(Q)$ of Eq. (2.16)$\propto Q^2$ as $Q\to0$, the leading terms of the renormalized quark loop ($n=2$ and 4) go as $1/R$. This leaves $\Gamma_{\rm kin}\propto R$ as the leading term, reflecting our choice $\mu_r^2=0$ for the renormalization point.

The behavior for small R, on the other hand, is determined by the short wavelength behavior of the n-point functions. In general, this depends on the regularization procedure, but for the case of $\Lambda=\infty$ we have from the Weinberg theorem [24] $F_2(Q)\to-(1/16\pi^2)\ln(Q^2/M^2)$ as $Q^2\to\infty$, and for $n>2$, $F_n(\lambda Q_1,\ldots,\lambda Q_n)\propto\lambda^{4-2n}$ as $\lambda\to\infty$. Therefore, for $\Lambda=\infty$ the $n=2$ term in Eq. (2.13) behaves as $\alpha M^2R\,\ln(MR)$ with $\alpha>0$, while the higher terms go as R^{n-1} ($n\geq4$). Since the $n=2$ term becomes negative and overshoots the kinetic term ($\Gamma_{\rm kin}\propto R$) for small R, the energy of the nontranslational invariant vacuum characterized by small sized meson configurations can become lower than the energy of the translational invariant vacuum.

If the regulator is kept finite, we can discuss the two terms $\overline{\Gamma_F}$ and $Z_M\Gamma_{\rm kin}$ in Eq. (2.11) separately. Since the unrenormalized two-point function $F_2(Q)$ of (2.15) vanishes for large Q as $1/Q^2$, at least in any regularization scheme which allows a dispersion representation for the two-point function, Γ_F gives terms of order R^3 or higher. Therefore the leading term in Eq. (2.11) goes as Z_MR. It follows that the translational invariant vacuum is stable if $Z_M>0$, but if $Z_M<0$ the vacuum instability occurs. (The case $\Lambda=\infty$ discussed above can be considered as a limiting case where $Z_M=-\infty$.)

Summarizing the above discussion, the vacuum part of the effective action (2.11) in the chiral symmetric nonlinear model behaves as

$$\Gamma_{\rm nl,vac}\to\Gamma_{\rm kin}+O(1/R)\quad(\text{large }R), \tag{2.17}$$

$$\Gamma_{\rm nl,vac}\to Z_M\Gamma_{\rm kin}+O(R^3)\quad(\text{small }R,\Lambda<\infty), \tag{2.18}$$

$$\Gamma_{\rm nl,vac}\to\alpha R\,\ln(MR)+O(R)\quad(\text{small }R,\Lambda=\infty), \tag{2.19}$$

[5]The general case is discussed in Appendix A.

[6]We will use capital (small) letters for Euclidean (Minkowski) four-momenta.

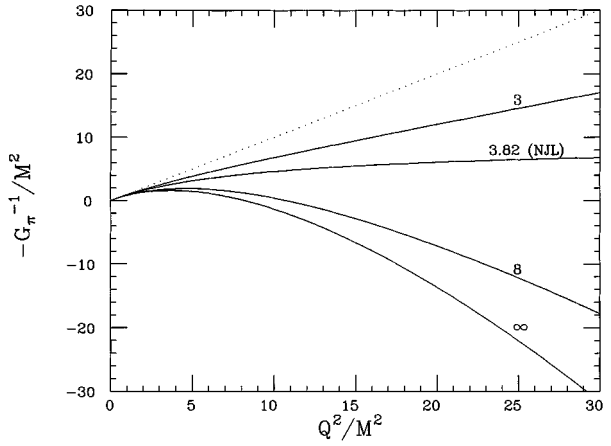

FIG. 1. The inverse SD pion propagator with $m_\pi=0$, $g=4$ for Euclidean Q^2. The numbers at the solid lines show the values of Λ/M, where Λ is the cutoff introduced in the dispersion integral. The case $\Lambda/M=3.82$ corresponds to the NJL model. The dotted line refers to $-G_\pi^{-1}=Q^2$, corresponding to $\Lambda/M=2$.

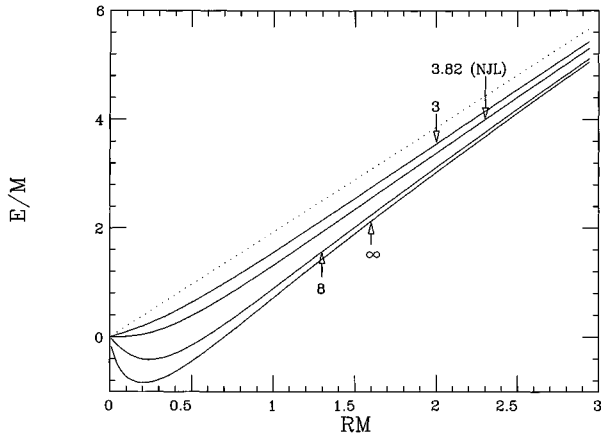

FIG. 2. The vacuum energy in the two-point approximation $[E=(1/T)\Gamma^{(2)}_{\rm nl,vac}]$ calculated using the exponential hedgehog profiles and the SD propagator shown in Fig. 1 in units of M as a function of MR. The numbers at the solid lines show the same values of Λ/M as in Fig. 1, and the case $\Lambda/M=3.82$ corresponds to the NJL model. The dotted line shows the kinetic energy, corresponding to $-G_\pi^{-1}=Q^2$ in Fig. 1.

with $\alpha>0$ and $\Gamma_{\rm kin}$ given by

$$\frac{1}{T}\,\Gamma_{\rm kin}=\frac{R}{2}\int\frac{d^3t}{(2\pi)^3}\,\mathbf{t}^2[s(\mathbf{t})s(-\mathbf{t})+\boldsymbol{\pi}(\mathbf{t})\cdot\boldsymbol{\pi}(-\mathbf{t})]. \tag{2.20}$$

In order to see the connection between the vacuum instability and the Landau ghost in the meson propagators more clearly, we will introduce the two-point approximation [25], which is obtained by keeping only the $n=2$ term in the quark loop (2.13). In this approximation, which includes the leading terms both for small and for large R, the vacuum effective action becomes

$$\frac{1}{T}\,\Gamma^{(2)}_{\rm nl,vac}=\frac{R}{2}\int\frac{d^3t}{(2\pi)^3}\,\mathbf{t}^2[s(\mathbf{t})s(-\mathbf{t})+\boldsymbol{\pi}(\mathbf{t})\cdot\boldsymbol{\pi}(-\mathbf{t})]\times\left[\frac{-G_\pi^{-1}(Q)}{Q^2}\right]_{Q=(0,\mathbf{t}/R)}, \tag{2.21}$$

where

$$-G_\pi^{-1}(Q)=Z_MQ^2+4g^2N_CQ^2\overline{F_2}(Q)=Q^2+4g^2N_CQ^2F_2(Q) \tag{2.22}$$

is the inverse Euclidean Schwinger-Dyson (SD) propagator of the pion in the one-quark-loop approximation. It behaves as Q^2 for small momenta, and as Z_MQ^2 [or $-Q^2\ln(Q^2/M^2)$ in the case of $\Lambda=\infty$] for large momenta:

$$Q^2(-G_\pi(Q^2))\to 1\quad\left(\frac{1}{Z_M}\right)\quad\text{as}\quad Q^2\to 0\quad(Q^2\to\infty). \tag{2.23}$$

Therefore, if $Z_M<0$ there must exist an Euclidean pole (Landau ghost) [11]. To illustrate the behavior of the pion propagator for various values of Λ, we use the dispersion regularization,[7] in which the dispersion integral for $\overline{F_2}$ is cut off at the invariant mass $\sigma^2=\Lambda^2$. Figure 1 shows the inverse pion propagator for $g=4$ ($M=372$ MeV) and various values of Λ, and Fig. 2 shows the corresponding behaviour of the vacuum energy (2.21) in the two-point approximation. Here we use the hedgehog fields with winding number one: $U=\exp[i\hat{\mathbf{r}}\cdot\boldsymbol{\pi}\Theta(r)\gamma_5]$ with the exponential profile $\Theta(r)=-\pi\exp(-r/R)$. The relation between the sign of Z_M, the Landau ghost and the vacuum instability can be clearly seen in these figures. In particular, there exists a ''critical'' cutoff Λ_c where $Z_M=0$. (In the present calculation $\Lambda_c/M=3.82$, which corresponds to an equivalent three-momentum cutoff of 605 MeV.) In this case, the pion propagator $G_\pi(Q)$ does not vanish for $Q^2\to\infty$ but rather goes to a constant [see Eq. (2.23) and Fig. 1], and the vacuum energy goes as R^3 for small R [see Eq. (2.18) and Fig. 2].

C. Ghost subtraction

If the pion self-energy in Eq. (2.22) satisfies a dispersion relation with a cut starting from $4M^2$, standard arguments [11,12] lead to the following dispersion representation of the SD propagator:[8]

[7]This regularization scheme is explained in Appendix B. It is equivalent to the three-momentum cutoff scheme if the loop momentum is cut off in a particular frame where the three-momentum of the meson is zero, and the result is generalized to an arbitrary frame [26].

[8]Our notation is such that the propagators for Euclidean and Minkowski momenta are related by $G_\pi(Q)\equiv G_\pi(q)|_{q^2=-Q^2}$. We also note that for finite Λ there may be branch points or poles above $4M^2$ in the dispersion integral in Eq. (2.24), i.e., the region of integration in Eq. (2.24) may split into several ones separated by regions with $\chi=0$, where the effect of the cut is effectively replaced by a Λ-dependent Minkowski pole with positive residue, cf. the discussion given below.

$$G_\pi(q) = \frac{1}{q^2 + i\epsilon} + \int_{4M^2}^{\infty} \frac{\chi(\sigma^2)}{q^2 - \sigma^2 + i\epsilon}\, d\sigma^2 + \Theta(\Lambda - \Lambda_c)\, \frac{Z_g}{q^2 + M_g^2} \tag{2.24}$$

with $\chi(\sigma^2) \geq 0$. The last term is the Landau ghost term with ghost mass M_g and residue $Z_g < 0$. Z_M can be expressed as [see Eq. (2.23)]

$$\frac{1}{Z_M} = 1 + \int_{4M^2}^{\infty} \chi(\sigma^2) d\sigma^2 + \Theta(\Lambda - \Lambda_c) Z_g . \tag{2.25}$$

We can use these expressions to discuss the behavior of the pion propagator shown in Fig. 1. (A more formal discussion is presented in Appendix B.) In the region $\Lambda > \Lambda_c$, where the Landau ghost exists, both the ghost mass M_g and the residue Z_g increase in magnitude without limits as we approach Λ_c from above ($\Lambda \to \Lambda_c + 0$). In this limit Z_M of Eq. (2.25) goes to zero and the ghost term in Eq. (2.24) goes to the (finite) q-independent value Z_g / M_g^2, i.e., the inverse Euclidean propagator becomes flat for $Q^2 \to \infty$:

$$\lim_{\Lambda \to \Lambda_c + 0} \frac{Z_g}{q^2 + M_g^2} = \left. \frac{Z_g}{M_g^2} \right|_{\Lambda = \Lambda_c} \equiv - \frac{1}{\mu^2} \tag{2.26}$$

with $\mu^2 > 0$. On the other hand, in the region $\Lambda < \Lambda_c$, where no Landau ghost exists, there must be a singularity in the integral (2.25) as we approach Λ_c from below ($\Lambda \to \Lambda_c - 0$), since Z_M vanishes in this limit. In Appendix B it is shown that this is due to a Minkowski pole term which replaces the cut for $\sigma^2 > \Lambda^2$. That is, $\chi(\sigma^2)$ consists of a smooth part $\Theta(\Lambda^2 - \sigma^2)\chi_0(\sigma^2)$ with χ_0 given by Eq. (B5), and a pole part $\Theta(\Lambda_c - \Lambda) Z_p \delta(\sigma^2 - M_p^2)$ with $M_p > \Lambda$, $Z_p > 0$. In the limit $\Lambda \to \Lambda_c - 0$, both M_p and Z_p diverge, but the pole term $Z_p / (q^2 - M_p^2 + i\epsilon)$ goes to the same finite constant as the ghost term, Eq. (2.26).

The ghost subtraction consists in replacing the SD propagator (2.24) by the KL propagator $\tilde{G}_\pi(q)$ which satisfies a KL representation and is related to the SD propagator by

$$\tilde{G}_\pi(q) = G_\pi(q) - \Theta(\Lambda - \Lambda_c)\, \frac{Z_g}{q^2 + M_g^2}. \tag{2.27}$$

The recipe of [11] to construct the new (ghost free) effective action is as follows: Take that part of the effective action which is quadratic in the meson fields, and replace its coefficient, which is the inverse SD propagator, by the inverse KL propagator. This prescription, which is *not* restricted to the two-point approximation, gives the following effective action:

$$\tilde{\Gamma} = \Gamma + \delta\Gamma, \tag{2.28}$$

$$\frac{1}{T}\, \delta\Gamma = \frac{1}{2} \int \frac{d^3 q}{(2\pi)^3} \left[s(\mathbf{q}) s(-\mathbf{q}) + \boldsymbol{\pi}(\mathbf{q}) \cdot \boldsymbol{\pi}(-\mathbf{q}) \right] \times \left[- \tilde{G}_\pi^{-1}(Q) + G_\pi^{-1}(Q) \right]_{Q = (0, \mathbf{q})} \tag{2.29}$$

This expression is valid also for the linear model [14]. Since the KL propagator satisfies the same renormalization conditions at zero momentum as the SD propagator, the behavior (2.17) of the vacuum effective action for large R is unchanged, while for small R the behavior is governed by a new wave function renormalization constant $\tilde{Z}_M$:

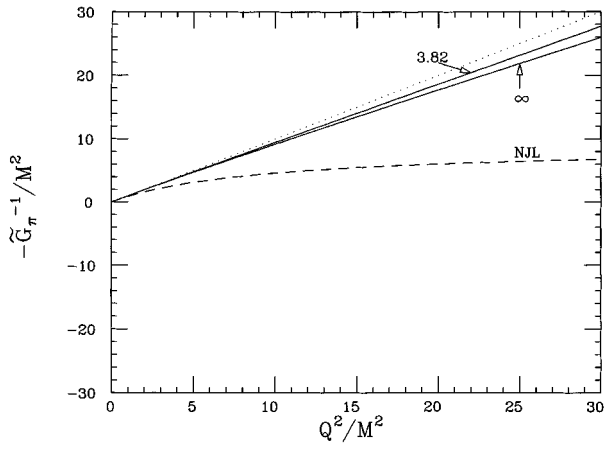

FIG. 3. The inverse KL pion propagator with $m_\pi = 0$, $g = 4$ for Euclidean Q^2. The numbers at the solid lines show the values of Λ/M. The solid line with $\Lambda/M = 3.82$ corresponds to the limit $\Lambda \to \Lambda_c + 0$. The dashed line shows the NJL result and is identical to the corresponding line in Fig. 1. The dotted line is the same as in Fig. 1.

$$\tilde{\Gamma}_{\mathrm{nl,vac}} \to \Gamma_{\mathrm{kin}} + O(1/R) \quad (\text{large } R), \tag{2.30}$$

$$\tilde{\Gamma}_{\mathrm{nl,vac}} \to \tilde{Z}_M \Gamma_{\mathrm{kin}} + O(R^3) \quad (\text{small } R), \tag{2.31}$$

with

$$\frac{1}{\tilde{Z}_M} = \lim_{Q^2 \to \infty} [-\tilde{G}_\pi(Q)] Q^2 = 1 + \int_{4M^2}^{\infty} \chi(\sigma^2) d\sigma^2. \tag{2.32}$$

Since $\tilde{Z}_M \geq 0$, it is clear that the ghost subtraction leads to a stable translational invariant vacuum. We note that for $\Lambda = \infty$ $\tilde{Z}_M$ is finite while Z_M diverges. In this case $\tilde{Z}_M = -1/Z_g$ due to Eq. (2.25).

We note, however, that the ghost subtraction inevitably introduces a discontinuity as Λ is varied across Λ_c: According to Eq. (2.26), the ghost term subtracted in Eq. (2.27), and therefore also $\delta\Gamma$ of Eq. (2.29), does not vanish for $\Lambda \to \Lambda_c + 0$, while for $\Lambda \to \Lambda_c - 0$ the ghost subtraction term is zero by definition. That is, the ''old'' theory for $\Lambda = \Lambda_c$ is reproduced by the ''new'' (ghost subtracted) theory in the limit $\Lambda \to \Lambda_c - 0$, but not in the limit $\Lambda \to \Lambda_c + 0$. The physical meaning of this will be discussed in the next subsection.

The KL pion propagator and the vacuum energy in the two-point approximation of the KL model $[(1/T)\tilde{\Gamma}^{(2)}_{\mathrm{nl,vac}}]$ which is obtained by replacing $G_\pi^{-1}(Q) \to \tilde{G}_\pi^{-1}(Q)$ in Eq. (2.21), are shown for $\Lambda > \Lambda_c$ by the solid lines in Figs. 3 and 4 for the same hedgehog profiles as before. The line $\Lambda/M = 3.82$ in Fig. 3 refers to the limit $\Lambda \to \Lambda_c + 0$. If Λ is increased to infinity, the inverse propagator varies smoothly between the two solid lines shown in this figure, i.e., after the

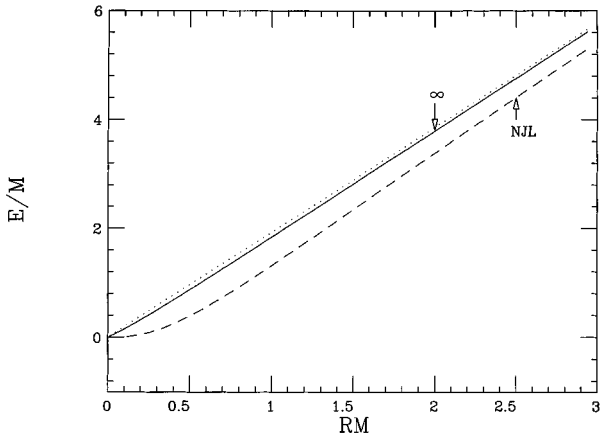

FIG. 4. The vacuum energy in the two-point approximation $[E=(1/T)\tilde{\Gamma}^{(2)}_{\rm vac}]$ calculated using the exponential hedgehog profiles and the KL propagator shown in Fig. 3 in units of M as a function of MR. The cutoff dependence for $\Lambda>\Lambda_c$ is too weak to be displayed on the scale used in this figure, and we show only the result for $\Lambda/M=\infty$ by the solid line. The dashed line shows the NJL result and is identical to the corresponding line in Fig. 2. The dotted line shows the kinetic energy as in Fig. 2.

ghost subtraction the cutoff dependence is very weak in the region $\Lambda>\Lambda_c$. The dashed line labeled by NJL refers to the limit $\Lambda\to\Lambda_c-0$ and is the same as the corresponding line in Fig. 1. For the vacuum energy shown in Fig. 4, the cutoff dependence in the region $\Lambda>\Lambda_c$ cannot be resolved on this scale, and therefore we show only the result for $\Lambda=\infty$. The dashed line is again the same as the NJL line of Fig. 2.

D. Connection to the NJL model

If we choose $m_\sigma^2=4M^2+m_\pi^2$ and $\Lambda=\Lambda_c$ in the linear σ model, the vacuum part (2.10) becomes[9]

$$\Gamma_{\rm vac}\big|_{\Lambda=\Lambda_c,m_\sigma^2=4M^2+m_\pi^2}=\overline{\Gamma}_F+\frac{v^2}{2}\,(m_\pi^2+\delta m_\pi^2)\times\int d^4x(U^+U-1)-c\int d^4x\sigma. \tag{2.33}$$

To see that this is just the effective action in the NJL model, it is convenient to return to the Lagrangian corresponding to Eq. (2.33), which has the form

$$\mathcal{L}^{(\rm NJL)}=\mathcal{L}_F+\frac{v^2}{2}\,\mu^2(U^+U-1)-\frac{m\mu^2}{g}\,\sigma, \tag{2.34}$$

where we defined the quantities μ^2 and m by

$$\mu^2=m_\pi^2+\delta m_\pi^2, \tag{2.35}$$

[9]Besides $Z_M=0$, this choice leads to a vanishing renormalization constant for the mesonic interactions [21,22] characterized by the coupling constant λ^2: $Z_\lambda=1+4M^2(Z_M-1)/(m_\sigma^2-m_\pi^2)=0$. It also leads to the relation $\lambda^2=2g^2$ (reduction of couplings [22]). We also notice that by including higher orders in $1/N_C$, the sigma mass in the NJL model becomes considerably smaller than $2M$ [22].

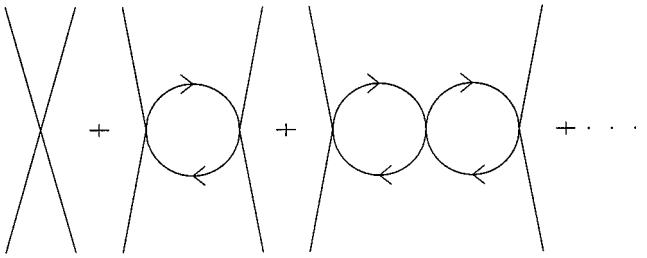

FIG. 5. Graphical representation of the $q\overline{q}\,t$ matrix in the NJL model.

$$\frac{m}{M}\,\mu^2=m_\pi^2\Rightarrow m=\frac{M}{1+\delta m_\pi^2/m_\pi^2}.$$

[Remember that $c=vm_\pi^2$, $M=gv$, and δm_π^2 is given by Eq. (2.8).] The Euler-Lagrange equations give immediately $\sigma=-(g/\mu^2)\psi\psi+m/g$, $\boldsymbol{\pi}=-i(g/\mu^2)\psi\boldsymbol{\tau}\gamma_5\psi$, and inserting these relations back into Eq. (2.34) one obtains the well-known NJL Lagrangian [16] with the four Fermi coupling constant $G=g^2/2\mu^2$ and the current u,d quark mass m. We therefore observe the following relation between the effective actions in the σ model and the NJL model on the one-quark-loop level:

$$\Gamma^{(\rm NJL)}=\Gamma\big|_{\Lambda=\Lambda_c,m_\sigma^2=m_\pi^2+4M^2}. \tag{2.36}$$

If we impose the condition $\sigma^2+\boldsymbol{\pi}^2=v^2$ and consider the chiral symmetric case, the whole discussion of Sec. II B can be applied to the NJL model by taking $\Lambda=\Lambda_c$ ($Z_M=0$). In particular, Eqs. (2.17)–(2.23) for $Z_M=0$ show that, due to the normalization conditions, the σ model (for any Λ) and the NJL model are equivalent for large sizes, but differ for small sizes. In particular, once we perform the ghost subtraction in the σ model, we expect from Eq. (2.31) that the NJL model gives lower soliton energies than the KL model, at least for small solitons.

The above discussion shows that for small R the NJL soliton is very soft with respect to changes in R: Since $Z_M=0$, its energy varies as R^3. In terms of the pion propagator, this means that the propagator in the NJL model does not vanish for large Q^2 but goes to a constant, see Eq. (2.23) and Fig. 1, and this constant was given in Eq. (2.26) in terms of the limiting values of the ghost mass and residue. If we approach the NJL model from above ($\Lambda\to\Lambda_c+0$), this constant is just subtracted in our KL propagator (2.27). That is, our KL propagator in the limit $\Lambda\to\Lambda_c+0$ behaves as $1/Q^2$ and has a finite Z_M (cf. the curve $\Lambda/M=3.82$ in Fig. 3). In order to understand the physical meaning of this relation,

$$G_\pi^{(\rm NJL)}(q)=G_\pi(q)\big|_{\Lambda=\Lambda_c}=\tilde{G}_\pi(q)\big|_{\Lambda=\Lambda_c+0}-\frac{1}{\mu^2}, \tag{2.37}$$

between the KL propagator and the NJL propagator, we recall the connection between $G_\pi^{(\rm NJL)}$ and the $q\overline{q}\,t$-matrix (see Fig. 5) in the NJL model:

$$t_\alpha(q)=\frac{2iG}{1+2G\overline{\Pi}_\alpha(q)}$$

$$\equiv ig[iG_\alpha^{(\mathrm{NJL})}(q)]ig \quad (\alpha=\sigma,\pi). \tag{2.38}$$

Here G is the four Fermi coupling constant, and $\overline{\Pi}_\alpha(q)$ is the bare bubble graph given by $\overline{\Pi}_\pi(q)=-4N_Cq^2F_2(q)-8N_cF_1$, $\overline{\Pi}_\sigma(q)=-4N_C(q^2-4M^2)F_2(q)-8N_cF_1$. Using the parameters g and μ^2, the NJL propagators can be rewritten into a form which also follows directly from Eq. (2.34):

$$G_\alpha^{(\mathrm{NJL})}(q)=\frac{-1}{\mu^2+g^2\overline{\Pi}_\alpha(q)}$$

$$\equiv\frac{-1}{m_\alpha^2+g^2\Pi_\alpha(q)} \quad [\Pi_\alpha(q)\equiv\overline{\Pi}_\alpha(q)-\overline{\Pi}_\alpha(0)]. \tag{2.39}$$

with $m_\pi^2=(m/M)\mu^2$, $m_\sigma^2=m_\pi^2+4M^2$ on account of Eq. (2.8) for $Z_M=0$, and the definition of μ^2 in Eq. (2.35).

Since the bare loop graphs $\Pi_\alpha(q)$ in a regularized model vanish for large Q^2, we see from Eq. (2.39) that the Euclidean propagators for large Q^2 go to $-1/\mu^2=-G/2g$. This just expresses the obvious fact that at short distance only the first term in Fig. 5 contributes. We therefore see that the ghost parameters of the σ model in the limit $\Lambda\to\Lambda_c+0$ are related to the four-Fermi coupling constant by Eq. (2.26). Moreover, from Eq. (2.37) it follows that our KL propagator (2.27) in the NJL limit ($\Lambda\to\Lambda_c+0$) reproduces the $q\overline{q}$ exchange chain graphs starting from the second diagram of Fig. 5. It is quite clear also intuitively that only these $q\overline{q}$ exchange diagrams correspond to the physical meson exchange described by the KL propagator $\widetilde{G}_\pi$, and that the first diagram of Fig. 5 should rather be interpreted as an interaction term peculiar to the NJL model, rather than part of a meson exchange process.

Summarizing, after ghost subtraction we have from Eq. (2.29) the following relation between the effective actions in the KL and the NJL model:

$$\Gamma^{(\mathrm{NJL})}=\widetilde{\Gamma}|_{\Lambda=\Lambda_c+0,\ m_\sigma^2=m_\pi^2+4M^2}$$

$$+\frac{T}{2}\int\frac{d^3q}{(2\pi)^3}[s(\mathbf{q})s(-\mathbf{q})+\boldsymbol{\pi}(\mathbf{q})\cdot\boldsymbol{\pi}(-\mathbf{q})]$$

$$\times[-G_\pi^{(\mathrm{NJL})^{-1}}(Q)+\widetilde{G}_\pi^{-1}(Q)|_{\Lambda=\Lambda_c+0}]_{Q=(0,\mathbf{q})}, \tag{2.40}$$

which replaces Eq. (2.36). Here the propagators $\widetilde{G}_\pi$ and $G_\pi^{(\mathrm{NJL})}$ are related by Eq. (2.37). The physical content of Eq. (2.40), which holds also in the linear model, is simple: The NJL model has an additional attractive point interaction $(-1/\mu^2)$ in the two-point function, while all higher-order Green's functions are the same. This additional attraction, given by the second term in Eq. (2.40), reduces the results shown by the upper solid line in Fig. 3 and the solid line in Fig. 4 to the NJL results shown by the dashed lines in these figures.

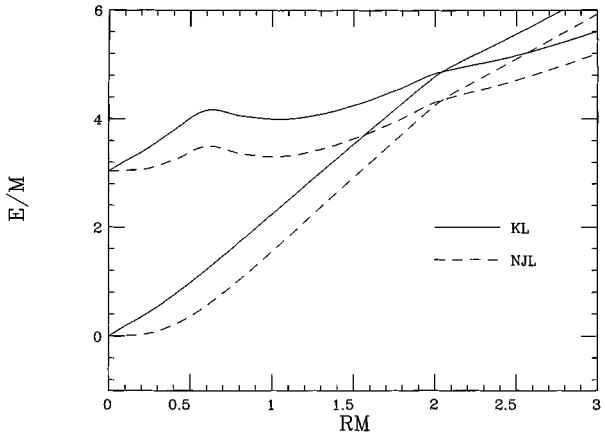

FIG. 6. The soliton energy calculated using the exponential hedgehog profiles in units of M as a function MR. The two lines starting from $E/M=0$ show the vacuum energy, and the two lines starting from $E/M=3$ show the total energy including the valence quark energy. The solid lines refer to the KL model with $\Lambda=\infty$, and the dashed lines to the NJL model.

III. NUMERICAL RESULTS

In this section we will discuss numerical results for the soliton energies and meson profiles obtained in the KL model and compare them with those obtained in previous work in the NJL model. Throughout this section we will refer to the chiral symmetric nonlinear model, i.e., $m_\pi=0$ and $\sigma^2+\boldsymbol{\pi}^2=v^2$. For the KL model, we will also restrict ourselves to the case $\Lambda=\infty$. The effective action for the KL model is then given by the vacuum part [Eq. (2.11)], the valence part and the ghost subtraction part (2.29). The fermion loop $\Gamma_F=\Gamma_F+$c.t. [see Eqs. (2.3) and (2.5)] is evaluated using a finite and discrete basis as explained in Sec. II A. In the NJL model, the vacuum part is simply the unrenormalized quark loop. To simplify comparisons with previous calculations for the NJL model in the literature [17], we will use the proper time regularization scheme. We will mainly refer to the case $g=4$, corresponding to a constituent quark mass $M=gf_\pi=372$ MeV.

First we discuss the results obtained for one-parameter profiles. Figure 6 shows the soliton energy as a function of the size R calculated with the exponential Hedgehog profiles in the KL model and in the NJL model. For each case, we show the vacuum energy and the total energy including the valence quark contribution. The vacuum energy in the KL model raises as $\widetilde{Z}_MR$ for small R [see Eq. (2.31)], with $\widetilde{Z}_M=0.65$ in our calculation. The total energy at the minimum at $R\simeq0.53$ fm is about $4M=1488$ MeV. Since the vacuum energy in the NJL model is characterized by $Z_M=0$ and raises as R^3 for small R, the energy in the NJL model has to lie below the KL result for small sizes. From the figure we see, however, that this holds also for medium sizes. For very large sizes, both models just reproduce the kinetic energy, see Eq. (2.30). The energy in the NJL model at the minimum $R\simeq0.53$ fm is about $3.3M=1228$ MeV. As we explained in detail in Sec. III, this difference of about $0.7M=260$ MeV can be attributed to the attractive contact $q\overline{q}$ interaction term (the first diagram in Fig. 5), which is absent in the KL model, see Eq. (2.40). Comparing Fig. 6 to Fig. 4,

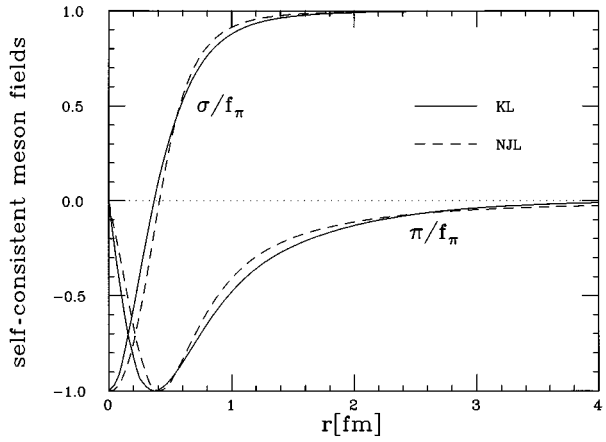

FIG. 7. The self-consistent σ and π fields obtained in the KL model (solid lines) and the NJL model (dashed lines).

we see that the small size approximation is quite accurate up to $RM \simeq 1$, but for larger sizes the vacuum energy is underestimated.

Next we discuss the results for self-consistent profiles. To calculate the chiral angle $\Theta(r)$ self-consistently, we write it as the sum of the exponential profile $\Theta_0 = -\pi \exp(-r/R)$ plus perturbation terms $a_n r^n \exp(-r/b_n)$ $(n=1,\ldots,N)$, and treat R, a_n and b_n as variational parameters. The actual calculation was performed with $N=7$–10, i.e., 15–21 parameters. The stability of the solution was checked by changing the starting values of these parameters, as well as by increasing N. For the NJL model our numerical procedure reproduced the results obtained by other authors.

The resulting self-consistent meson fields for the KL and the NJL model are shown in Fig. 7. Although the fields in the KL model are similar to those in the NJL model, we note that in the NJL model they are somewhat more localized. The fact that the fields in the KL model tend to avoid curvatures can readily be understood from Eq. (2.21), which shows that in the KL model the high momentum components of the fields are weighted by $\tilde{Z}_M Q^2$, while in the NJL model they are weighted by a constant.

The results for the soliton energies in the KL and NJL models are shown in Table I for the coupling constants $g=4$ and 5. We see that the valence quark energies are rather similar in the KL and NJL model, which reflects the similarity of the self-consistent fields. The vacuum energies in the KL model are much larger than in the NJL model. Again we note that this is due to the additional attractive qq contact interaction in the NJL model represented by the first diagram in Fig. 5 or the second term in Eq. (2.40).

TABLE I. The soliton (hedgehog) energies (in MeV) obtained in the KL model and the NJL model for the couplings $g=4$ and 5. The results are split into the valence quark contribution and the vacuum contribution.

g	$E_{\rm val}$	$E_{\rm vac}$	$E_{\rm tot}$
	KL model		
4	639	845	1484
5	439	1064	1503
	NJL model		
4	628	586	1214
5	457	740	1197

Let us compare these results to the two-point approximation discussed in Sec. II and to calculations where the Dirac sea has been neglected [6]:[10] As we can expect from Fig. 4, the effect of the Dirac sea in the two-point approximation to the KL model gives only a very small attraction. Indeed, a self-consistent calculation within the two-point approximation leads to results which are very similar to those of [6]: The hedgehog energies are 1280 MeV (1108 MeV) for $g=4$ ($g=5$), compared to the value 1115 MeV of [6] obtained for $g=5.28$. The mean meson fields obtained in the two-point approximation are also very similar to those of [6], and show a larger spatial extension than those of Fig. 7. As we have seen earlier, however, the full quark loop deviates from the two-point approximation for $RM>1$, where it gives a strongly repulsive contribution. This leads to considerably higher hedgehog energies and to narrower mean fields in the full calculation.

The fact that the soliton energies in the KL model are considerably larger than the average mass of the nucleon and the delta seems to indicate that the restriction of the fields on the chiral circle is not justified, and for quantitative purposes it is therefore important to perform the calculations in the linear model. For the linear NJL model it is well known that there exist no stable solitonic solutions [18,19]. It has actually been shown numerically in [19] that in the limit of small sizes $(R\to 0)$ and deep fields $(U\to\infty)$, but with UR^α kept fixed, the unrenormalized fermion loop Γ_F and also the total energy in the NJL model go to zero for $1<\alpha<3/2$. It has already been pointed out [28] that a repulsive term of fourth order in the fields can cure this instability, since this term goes to infinity as $R^{3-4\alpha}$ in the above limit.[11] Besides such a term, which is present in the linear KL model with variable strength characterized by m_σ^2, the KL model in the small size limit also contains the meson kinetic term, which goes as $\tilde{Z}_M R^{1-2\alpha}$ and therefore also avoids the collapse. One can therefore expect that stable solitonic solutions exist in the linear KL model.

IV. SUMMARY AND CONCLUSIONS

In this paper we investigated solitonic solutions with baryon number 1 in the chiral σ model. It is well known that after renormalization this model suffers from an instability of the translational invariant vacuum if the cutoff exceeds some critical value, and that this instability is due to an unphysical tachyon pole (Landau ghost) in the meson propagators. To cure this instability, while remaining in the one-loop ap-

[10]The calculations of [6] are performed in the linear model, but since a rather large σ mass is used, the deviations from the chiral circle are small.

[11]Also other methods to cure the instability of the linear NJL model have been proposed: The instanton induced 6-fermi interaction [18], a regularization scheme for the (constrained) baryon number [29], and vector mesons [30].

proximation, we have introduced the KL model, in which, by construction, the meson propagators satisfy the KL representation and are free of the Landau ghost. Our work serves two purposes: First, to clarify the connection of the KL model to the NJL model, and, second, to present solitonic solutions in the KL model for the case where the meson fields are on the chiral circle (nonlinear model). We can summarize the results as follows.

First, the NJL and KL models are equivalent for long meson wavelengths (large sizes), but differ for short meson wavelengths (small sizes). For small sizes, the effective action (energy) in the original σ model is dominated by the kinetic energy of the unrenormalized meson fields, which behaves as $Z_M\mathbf{q}^2$ with $|\mathbf{q}|$ some momentum characteristic for the Fourier components of the fields. Since the bosonized NJL model has no explicit mesonic kinetic term in the effective action, it is characterized by $Z_M=0$. One can, however, choose the cutoff in the σ model such that $Z_M=0$, and then the NJL model is simply a particular case of the σ model with the cutoff $\Lambda=\Lambda_c$ (and sigma mass $m_\sigma^2=4M^2+m_\pi^2$). In the σ model, however, Z_M can become negative, which leads to the Landau ghost and the vacuum instability discussed above. In this case, which happens for $\Lambda>\Lambda_c$, one has to introduce a ghost subtraction term into the effective action, i.e., one must employ the KL model. As we have shown in detail, this ghost subtraction term survives even in the NJL limit $\Lambda\to\Lambda_c+0$, in which case it removes the short range part of the $q\overline{q}$ interaction (the first diagram in Fig. 5). The difference between the NJL and the KL model is then that the former includes this pointlike $q\overline{q}$ interaction and the latter does not. We have noted that by subtracting this contact interaction one effectively obtains a kinetic term $\propto\widetilde{Z}_M R$ for small solitons with $\widetilde{Z}_M>0$. This term is expected to avoid the collapse observed in the linear NJL model for small sizes and deep fields. For large soliton sizes, the two models are still equivalent to each other due to the imposed renormalization conditions. We also pointed out that, once the ghost is subtracted, the cutoff dependence in the nonlinear KL model is rather weak, and therefore we limited our self consistent calculations to the case $\Lambda=\infty$.

Second, the self-consistent meson fields in the KL model are quite similar to those in the NJL model. Since the KL model can be thought of as the NJL model without the attractive $q\overline{q}$ point interaction, the soliton masses in the KL model are considerably larger than those in the NJL model (about four times the constituent quark mass). That is, in the nonlinear KL model one will not be able to reproduce the nucleon and the delta masses, and therefore the calculations should be done in the linear model. On the basis of the present work, it remains to be seen whether the linear KL model can successfully describe the baryon properties or not.

ACKNOWLEDGMENTS

One of the authors (W.B.) wishes to thank Dr. K. Tanaka for helpful discussions. W.B. was supported by the Grant in Aid for Scientific Research of the Japanese Ministry of Education, Project No. C-07640383. J.H. was supported by Deutsche Forschungsgemeinschaft under Contract No. BE 348/11-1,2.

APPENDIX A: SMALL SIZE EXPANSION AND TWO-POINT APPROXIMATION OF THE QUARK LOOP PART

The small size expansion of $\Gamma_F=\overline{\Gamma_F}+\text{c.t.}$ [see Eqs. (2.3) and (2.5)] corresponds to an expansion in terms of n-point functions with vertices described by V of Eq. (2.4). If we express $\Gamma_F=\Sigma_{n=2}^{\infty}(-1)^n/2n\ \mathrm{Tr}[(GV)^n-\delta_{n,2}G^2V^2]$ in a plane wave basis, we obtain for time independent meson fields in the continuum limit

$$\frac{1}{T}\Gamma_F=N_C\sum_{n=2}^{\infty}\frac{(-1)^n}{2n}\int\frac{d^3q_1}{(2\pi)^3}\cdots\frac{d^3q_{n-1}}{(2\pi)^3}\,\mathrm{tr}[V(\mathbf{q}_1)\cdots V(\mathbf{q}_n)][\overline{F_n}(Q_1,\ldots,Q_{n-1})|_{Q_i=(0,\mathbf{q}_i)}-\delta_{n,2}\overline{F_2}], \tag{A1}$$

where $V(\mathbf{q})$ is the three-dimensional Fourier transform of $V(\mathbf{r})$, the unrenormalized n-point functions are given by Eq. (2.15), and F_2 by Eq. (2.9). Assuming that the meson fields depend only on $\mathbf{x}=\mathbf{r}/R$, and introducing $\mathbf{t}=\mathbf{q}R$, we have from Eq. (2.4)

$$V(\mathbf{q})=R^2[V_1(\mathbf{t})+RV_2(\mathbf{t})]\equiv R^2V(\mathbf{t}) \tag{A2}$$

with $V_1(\mathbf{t})$ given in Eq. (2.14), and

$$V_2(\mathbf{t})=g^2\left[2vs(\mathbf{t})+\int d^3x e^{i\mathbf{t}\cdot\mathbf{x}}[s^2(\mathbf{x})+\boldsymbol{\pi}^2(\mathbf{x})]\right]. \tag{A3}$$

In terms of the variables $\mathbf{t}_i$, we arrive at Eq. (2.13) with $V_1(\mathbf{t})$ replaced by $V(\mathbf{t})$. [Note that Eq. (2.13) applies to the nonlinear model where $V_2=0$.]

The two-point approximation consists in keeping only the $n=2$ term in Γ_F. After adding the mesonic terms Γ_M and Γ_{SB}, we obtain

$$\frac{1}{T}\Gamma^{(2)}_{\rm vac}=\frac{R}{2}\int\frac{d^3t}{(2\pi)^3}\,\mathbf{t}^2\left\{\boldsymbol{\pi}(\mathbf{t})\cdot\boldsymbol{\pi}(-\mathbf{t})\left[\frac{-G_\pi^{-1}(Q)}{Q^2}\right]+s(\mathbf{t})s(-\mathbf{t})\left[\frac{-G_\sigma^{-1}(Q)}{Q^2}\right]\right\}_{Q=(0,\mathbf{t}/R)}+\frac{R^3}{2}g^2\int\frac{d^3t}{(2\pi)^3}\,[4vs(\mathbf{t})\tilde{V}_2(-\mathbf{t})$$
$$+\tilde{V}_2(\mathbf{t})\tilde{V}_2(-\mathbf{t})]\left[\frac{m_\sigma^2-m_\pi^2}{4M^2}+4g^2N_CF_2(Q)\right]_{Q=(0,\mathbf{t}/R)}. \tag{A4}$$

Here the inverse Euclidean propagators are given by ($\alpha=\sigma,\pi$)

$$-G_\alpha^{-1}(Q)=m_\alpha^2+Z_MQ^2+4g^2N_CQ^2\overline{F_2}(Q)+\delta_{\alpha,\pi}16g^2N_CM^2F_2(Q)$$
$$=m_\alpha^2+Q^2+4g^2N_CQ^2F_2(Q)+\delta_{\alpha,\pi}16g^2N_CM^2F_2(Q). \tag{A5}$$

In Eq. (A4), the contribution from the first term in V_2 of Eq. (A3) is included in the σ propagator, and the rest is denoted as $g^2\tilde{V}_2(\mathbf{t})$, i.e., $\tilde{V}_2(\mathbf{t})$ is the Fourier transform of $s^2(\mathbf{x})+\boldsymbol{\pi}^2(\mathbf{x})$.

APPENDIX B: PION PROPAGATOR IN THE DISPERSION REGULARIZATION SCHEME

The dispersion regularization scheme consists in cutting off the dispersion integral for the two-point function[12] $F_2(q)$ in Eq. (2.22) at $\Lambda^2>4M^2$:

$$\overline{F_2}(q)=\int_{4M^2}^{\Lambda^2}\frac{\rho(\sigma^2)d\sigma^2}{\sigma^2-q^2-i\epsilon},$$

$$\rho(\sigma^2)=\frac{1}{16\pi^2}\sqrt{1-\frac{4M^2}{\sigma^2}}. \tag{B1}$$

We have $Z_M=1-4g^2N_C\overline{F_2}>0(<0)$ if $\Lambda<\Lambda_c(\Lambda>\Lambda_c)$. [Here $F_2\equiv F_2(0)$.] The pion propagator $G_\pi(q)=[Z_Mq^2+4g^2q^2N_CF_2(q)]^{-1}$ for exact chiral symmetry has the pion pole at $q^2=0$. The other poles are determined from

$$4g^2N_C\overline{F_2}(q)=-Z_M. \tag{B2}$$

Consider first the case $\Lambda<\Lambda_c$, where $Z_M>0$. Then Eq. (B2) has a solution for $q^2\equiv M_p^2>\Lambda^2$ with residue $Z_p>0$:

$$4g^2N_C\int_{4M^2}^{\Lambda^2}\frac{\rho(\sigma^2)d\sigma^2}{M_p^2-\sigma^2}=Z_M,$$

$$Z_p=\left[4g^2N_CM_p^2\int_{4M^2}^{\Lambda^2}\frac{\rho(\sigma^2)d\sigma^2}{(M_p^2-\sigma^2)^2}\right]^{-1}. \tag{B3}$$

We therefore have the following spectral representation of the pion propagator for $\Lambda<\Lambda_c$:

$$G_\pi(q)=\frac{1}{q^2+i\epsilon}+\int_{4M^2}^{\infty}\frac{\chi_0(\sigma^2)}{q^2-\sigma^2+i\epsilon}\,d\sigma^2+\frac{Z_p}{q^2-M_p^2+i\epsilon}. \tag{B4}$$

Here

$$\chi_0(q^2)=\frac{-1}{\pi}\frac{\mathrm{Im}\,g^2\Pi_\pi(q)}{[q^2-\mathrm{Re}\,g^2\Pi_\pi(q)]^2+[\mathrm{Im}\,g^2\Pi_\pi(q)]^2} \tag{B5}$$

with $\Pi_\pi(q)=-4q^2N_C[\overline{F_2}(q)-\overline{F_2}]$. It is easy to see from Eq. (B3) that for $\Lambda\to\Lambda_c-0$ ($Z_M\to+0$) we have $M_p^2\to\infty$, $Z_p\to\infty$ such that the pole term in Eq. (B4) becomes in this limit

$$\frac{Z_p}{q^2-M_p^2}\to\frac{-Z_p}{M_p^2}=-\left[4g^2N_C\int_{4M^2}^{\Lambda_c^2}\rho d\sigma^2\right]^{-1}. \tag{B6}$$

As we explained in Sec. II, this limit is just $-1/\mu^2=-2G/g^2$. Turning now to the case $\Lambda>\Lambda_c$, where $Z_M<0$, Eq. (B2) has a solution for $q^2=-M_g^2<0$ with residue $Z_g<0$ (Landau ghost). With the replacements $Z_p\to Z_g$, $M_p^2\to-M_g^2$, the same relations (B3)–(B6) hold, except that there is no $i\epsilon$ in the denominator of the ghost pole term.

[12] For the formulas in this appendix we use the Minkowski four momentum q.

[1] G. 't Hooft, Nucl. Phys. **B72**, 461 (1974); E. Witten, *ibid*. **160**, 57 (1979); **B223**, 422 (1983); **B223**, 433 (1983).

[2] R. Friedberg and T. D. Lee, Phys. Rev. D **15**, 1694 (1977); **18**, 2623 (1978).

[3] L. Wilets, *Nontopological Solitons* (World Scientific, Singapore, 1989), Vol. 24.

[4] M. Gell-Mann and M. Lévy, Nuovo Cimento **16**, 705 (1960); B. W. Lee, *Chiral Dynamics* (Gordon and Breach, New York, 1972).

[5] S. Kahana, G. Ripka, and V. Soni, Nucl. Phys. **A415**, 351 (1984).

[6] M. C. Birse and M. K. Banerjee, Phys. Rev. D **31**, 118 (1985).

[7] G. Ripka and S. Kahana, Phys. Rev. D **36**, 1233 (1987).

[8] R. Perry, Phys. Lett. B **199**, 489 (1987); V. Soni, *ibid*. **183**, 91

(1987); T. D. Cohen, M. K. Banerjee, and V-Y. Ren, Phys. Rev. C **36**, 1653 (1987).
[9] T. Muta, *Foundations of Quantum Chromodynamics* (World Scientific, Singapore, 1987), Sec. 3.3.2.
[10] L. D. Landau, in *Niels Bohr and the Development of Physics*, edited by W. Pauli (Pergamon, London, 1955).
[11] K. Tanaka, W. Bentz, A. Arima, and F. Beck, Nucl. Phys. **A528**, 676 (1991).
[12] P. J. Redmond, Phys. Rev. **112**, 404 (1958); N. N. Bogoliubov, A. A. Logunov, and D. V. Shirkov, Sov. Phys. JETP **37**, 574 (1960).
[13] S. H. Kahana and G. Ripka, Phys. Lett. B **278**, 11 (1992).
[14] J. Hartmann, F. Beck, and W. Bentz, Phys. Rev. C **50**, 3088 (1994).
[15] K. Tanaka and W. Bentz, Nucl. Phys. **A540**, 383 (1992); G. Hejc, W. Bentz, and H. Baier, *ibid*. **A582**, 401 (1995).
[16] Y. Nambu and G. Jona-Lasinio, Phys. Rev. **122**, 345 (1961); **124**, 246 (1961).
[17] H. Reinhardt and R. Wünsch, Phys. Lett. **230**, 93 (1989); M. Wakamatsu and H. Yoshiki, Nucl. Phys. **A524**, 561 (1991); Th. Meissner, F. Grümmer, and K. Goeke, Ann. Phys. **202**, 297 (1990).
[18] M. Kato, W. Bentz, K. Yazaki, and K. Tanaka, Nucl. Phys. **A551**, 541 (1993).
[19] P. Sieber, Th. Meissner, F. Grümmer, and K. Goeke, Nucl. Phys. **A547**, 459 (1992).
[20] W. Bentz, Prog. Nucl. Part. Phys. **36**, 179 (1996).
[21] T. Eguchi, Phys. Rev. D **17**, 611 (1978); K. Shizuya, *ibid*. **21**, 2327 (1980).
[22] F. Cooper and J. Perez-Mercader, Phys. Rev. D **43**, 4129 (1991); D. Lurie and G. B. Tupper, *ibid*. **47**, 3580 (1993); K. Akama, Phys. Rev. Lett. **76**, 184 (1996).
[23] W. Bentz, L. G. Liu, and A. Arima, Ann. Phys. **188**, 61 (1988).
[24] C. Itzykson and J.-B. Zuber, *Quantum Field Theory* (McGraw-Hill, New York, 1985).
[25] I. Adjali, I. J. R. Aitchison, and J. A. Zuk, Nucl. Phys. **A537**, 457 (1992).
[26] T. Hatsuda and T. Kunihiro, Phys. Rep. **247**, 221 (1994).
[27] S. Kahana and G. Ripka, Nucl. Phys. **A429**, 462 (1984).
[28] C. Weiss, R. Alkhofer, and H. Weigel, Mod. Phys. Lett. A **8**, 79 (1993).
[29] J. Schlienz, H. Weigel, H. Reinhardt, and R. Alkhofer, Phys. Lett. B **315**, 6 (1993).
[30] E. Ruiz Arriola, F. Döring, C. Schüren, and K. Goeke, J. Phys. G **20**, 399 (1994).